# Detection and classification of skylights on the flank of Elysium Mons, Mars

Ravi Sharma[1] and Neeraj Srivastava[2]

[1]J.J.T. University, Jhunjhunu, Rajasthan 333001, India
[2]Planetary Science Division, Physical Research Laboratory, Ahmedabad 380009, India

November 18, 2022

## Abstract

The Martian caves have revived interest in the field of speleology because they are the potential destinations for future human residences and astrobiological research. The skylights are formed by the collapse of the surface materials into the subsurface void spaces. Hence, they are the doors to access the subsurface caves. The signature of life is probable in a sub-surface cave on Mars as it can protect life from the harsh and dangerous radiation environment of the surface. In a cave, there may be an abundance of minerals, fluids, and other key resources. Therefore, locating the skylights is essential and crucial for formulating plans for robotics/human explorations of the Red Planet, Mars. We have used remote sensing data from MRO (Mars Reconnaissance Orbiter; NASA), MGS (Mars Global Surveyor; NASA), and Mars Odyssey (NASA) for identifying, mapping, and classifying of skylights based on their morphology, morphometry, and thermal behavior. A total of thirty-two skylight candidates have been examined which includes twenty-six newly discovered ones. Out of these, seventeen have been classified as Atypical Pit Craters (APCs) and fifteen as Bowl-shaped Pit Craters (BPCs). Among these, there are twelve newly found APCs. The APCs are considered as potential skylights associated with caves; however, considering the formation and the geological context, fifteen BPCs, which have displayed the requisite morphological and thermal behavior, have also been considered as potential skylights.

# Detection and classification of skylights on the flank of Elysium Mons, Mars

Ravi Sharma[1], Neeraj Srivastava[2],

[1]J.J.T. University, Jhunjhunu, Rajasthan 333001, India

[2]Planetary Science Division, Physical Research Laboratory, Ahmedabad 380009, India

Corresponding author: Ravi Sharma (ravisharma.rs08@gmail.com)

Corresponding author: Neeraj Srivastava (sneeraj@prl.res.in)

**Key Points:**

- Twenty-six new potential skylights have been discovered in the Elysium Mons region
- A total of thirty-two skylight candidates have been classified based upon morphometry and geological context
- Potential cave entrances have been detected using the HiRISE camera onboard MRO

**Abstract:** The Martian caves have revived interest in the field of speleology because they are the potential destinations for future human residences and astrobiological research. The skylights are formed by the collapse of the surface materials into the subsurface void spaces. Hence, they are the doors to access the subsurface caves. The signature of life is probable in a sub-surface cave on Mars as it can protect life from the harsh and dangerous radiation environment of the surface. In a cave, there may be an abundance of minerals, fluids, and other key resources. Therefore, locating the skylights is essential and crucial for formulating plans for robotics/human explorations of the Red Planet, Mars. We have used remote sensing data from MRO (Mars Reconnaissance Orbiter; NASA), MGS (Mars Global Surveyor; NASA), and Mars Odyssey (NASA) for identifying, mapping, and classifying of skylights based on their morphology, morphometry, and thermal behavior. A total of thirty-two skylight candidates have been examined which includes twenty-six newly discovered ones. Out of these, seventeen have been classified as Atypical Pit Craters (APCs) and fifteen as Bowl-shaped Pit Craters (BPCs). Among these, there are twelve newly found APCs. The APCs are considered as potential skylights associated with caves; however, considering the formation and the geological context, fifteen

BPCs, which have displayed the requisite morphological and thermal behavior, have also been considered as potential skylights.

**Plain Language Summary:** The present-day environment of the surface of Mars is very harsh and inadequate for life to exist due to extreme temperature variations, dust storms, high UV, and cosmic rays. However, today life can survive and be found in the subsurface environment of Mars such as in the caves where key resources may also be present. Skylights that form by the collapse of the roof are potential indicators of caves on Mars therefore locating them is essential and crucial for formulating plans for robotics/human explorations of the Red Planet, Mars. In this study, we have examined a total of thirty-two skylight candidates in the Elysium Mons region for morphology, morphometry, and thermal behavior using remote sensing data from MRO (Mars Reconnaissance Orbiter; NASA), MGS (Mars Global Surveyor; NASA), and Mars Odyssey (NASA). Out of these seventeen have been classified as Atypical Pit Craters (APCs). Besides, their geological setting has been studied and potential entrances have been worked out for the candidates for which HiRISE data was available. It has been found that two of the skylight candidates are associated with lava tubes and three with tectonic features. Others could be associated with horizontal magma conduits.

## 1. Introduction

A skylight is an opening of the cave roof or ceiling to admit the natural light. The skylights are cave entrances that are formed by the collapse of surface material into the subsurface void spaces. They can be associated with tube-fed lava flows, volcanic-tectonic features, or rille structures (Cushing et al., 2012; 2015). The skylight forms by the collapse of the upper cave roof into the void space. The sunlight enters the cave entrance zone from the skylight and very high-temperature fluctuation occurs in the portion that is directly illuminated. The surrounding areas in the twilight zone exhibit only minor temperature changes because they are illuminated only by scattered light. Most importantly, the temperature in the un-illuminated part of the cave remains constant. So, there is the possibility of an abundance of ice and other cave resources (Boston et al., 2003a, 2003b; Hill et al., 1997; Romero, 2009; Bairagya, 2014). Apart from these, the caves also protect from dust storms, high ultraviolet radiations, and cosmic rays

(Boston et al., 2004). Thus, the caves are the potential sites for future robotics/human explorations of the surface of Mars (Boston et al., 2003b). Considering these aspects in this study, we have explored skylights in the Elysium Mons region of Mars (Fig.1 (iii) with the help of existing datasets from various remote sensing missions.

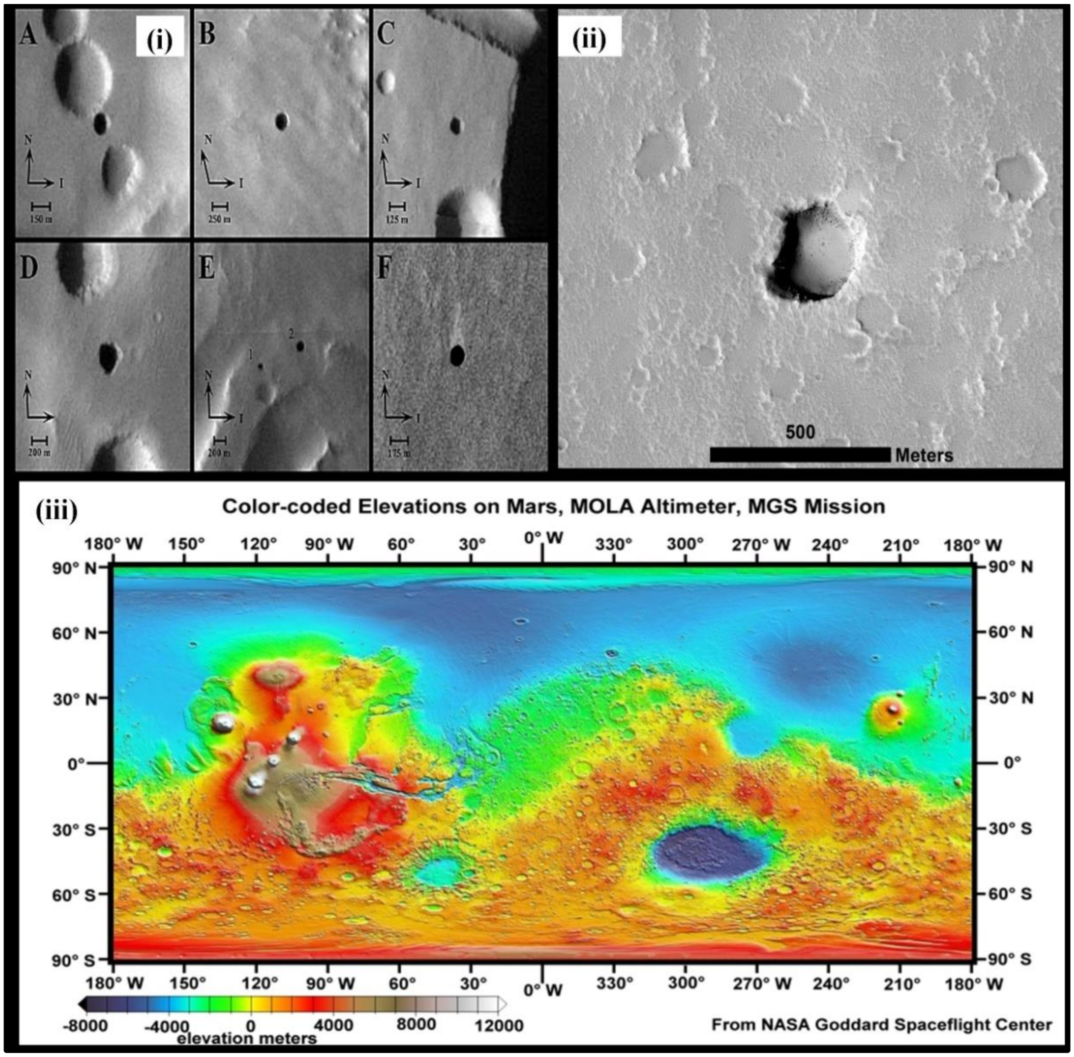


**Fig. 1:** (i) The Seven Sisters on Mars (Cushing, 2007); (ii) The first skylight reported from the Elysium region by Cushing et al. (2015); (iii) A MOLA data derived elevation map of Mars (MOLA team, NASA Goddard Space Flight Centre, 2003) (Web link - https://www.lpi.usra.edu/science/treiman/greatdesert/workshop/marsmaps1/) showing Arsia Mons, where the seven sisters are located and the Elysium Mons region, which is the region of interest in the present study.

The skylights were discovered on Mars in the year 2007 in the Tharsis region (Cushing et al., 2007). These constitute the seven skylight candidates (Fig.1 (i)) on the flank of the Arsia Mons (Fig.1 (iii)) popularly known as *Seven Sisters on Mars*. Several skylights were found in the Tharsis region after that; however, the first skylight in the Elysium region (Fig.1 (ii)) was spotted only very recently by Cushing et al. (2015). Cushing (2019) has released an updated version of the Mars Cave Candidate Catalog, which includes forty-four skylights present on the flank of the Elysium Mons. Out of these, we have included six skylight candidates in this study for detailed morphometry and thermal examination. In addition to these, in this study, we have searched for new skylights in the Elysium Mons region of Mars using remote sensing datasets from Mars Reconnaissance Orbiter (MRO), Mars Global Surveyor (MGS), and Mars Odyssey missions of NASA.

## 2. Datasets Used

In this study, we have used imaging datasets, spectrometer data, and altimetry data from several remote sensing missions to Mars by NASA. These include panchromatic data from High-Resolution Imaging Science Experiment (HiRISE) and ConTeXt (CTX) camera from Mars Reconnaissance Orbiter (MRO; 2005-present) (Malin et al., 2007), and THEMIS Infrared Projected Brightness Temperature Image (IRPBT) data from Mars Odyssey (NASA) (Christensen et al., 2004; 2017) downloaded through the publically accessible web portal - Mars Orbital Data Explorer (ODE) (https://ode.rsl.wustl.edu/mars/) produced by the PDS Geosciences Node at Washington University in St. Louis. We have also used Mars Orbiter Laser Altimeter (MOLA) data from Mars Global Surveyor (NASA) (Smith et al., 2001; 2003) (Web link - ftp://pdsimage2.wr.usgs.gov/pub/pigpen/mars/mola/mola128_88Nto88S_Simp_clon0.zip). The spatial resolutions for these datasets are 0.25m/pixel for HiRISE, ~ 5-6 m/pixel for CTX, ~ 100 m/pixel for THEMIS IRPBT, and ~ 463 m/pixel for MOLA DEM. The THEMIS IRPBT data is computed from Band 9 (12.57 µm) calibrated spectral radiance values assuming atmospheric opacity of 0.0 and surface emissivity of 1.0 (Christensen et al., 2017). Apart from this, we have used geological unit layers from Tanaka et al. (2014) (Web link - http://pubs.usgs.gov/sim/3292), and Mars Cave Catalog from Cushing and Okubo (2015), and Cushing (2019) (https://www.sciencebase.gov/catalog/item/5bd36eb1e4b0b3fc5ce51783).

## 3. Methodology

### 3.1 Identification of skylight candidates

Initially, CTX and/or HiRISE images have been used to detect skylight candidates based upon morphological investigations. As viewed from the orbit, the skylight occurs as a mostly circular structure having a collapsed cave roof and exhibiting shadowed appearance in the un-illuminated part (Cushing et al., 2015). Unlike any impact craters, they are devoid of elevated rims, ejecta blanket, and rays (Fig. 2). Further, the skylights show a warmer appearance than the surrounding area at night time (Cushing et al., 2015; Jung et al., 2014; Sharma et al., 2019) because the heat from the outer surface is easily radiated towards space while the loss of heat stored inside a cave is greatly inhibited and the cave radiates most of the heat energy through the skylights in the night time (Antoine et al., 2009, 2011; Lopez et al., 2012).

Therefore, in this study, we have used the night time THEMIS IR data of the northern summer season (Solar Longitude; Ls 90-180) for thermal observations. Here, "THEMIS IR" refers to the THEMIS Band-9 data (centered at 12.57 μm). Band-9 is useful because it detects surface brightness temperatures at a high signal-to-noise ratio (SNR) even at low temperatures. It is appropriate to use the midnight data of the THEMIS IR observations because, at that time, the difference in the temperature of the skylight and the temperature of the surrounding area is maximum. In this study, we have restricted the extent of the surrounding area to a circular buffer zone of a radius of 500 m. The mid-nighttime temperature difference of the surrounding region (radius 500 m) of a skylight candidate $T_D$ has been calculated by estimating the difference between the candidate skylight point location night-time maximum temperature ($T_{max}$) and their average surrounding (radius 500 m) temperature ($T_{mean}$). While estimating $T_{mean}$ the temperature of the hotter pixel/pixels has not been included. In most of the cases, we have carried out thermal observations around midnight time from ~ 23:30 to 2:00. The thermal observation data of night time ~ 21:00 to 22:00 has been used in a few cases where midnight data was not available. The skylight shows a warmer appearance than the surrounding area, if $T_D > 0$. Apart from these, the temperature of the potential cave floor fluctuates with much lower diurnal amplitudes than the nearby surfaces (Cushing et al., 2015). Therefore, we have calculated the diurnal amplitudes of the skylight candidate point location and the surrounding region. For this, $T_{max}$, $T_{mean,}$ and $T_D$ have been calculated for the thermal observations during the day (D) as well, ~13:00-14:00. Here, it is important to mention that the temperature data of the daytime and the nighttime for different skylight candidates are not corresponding to the same day on Mars.

## 3.2 Classification of Skylight Candidates

### 3.2.1 Morphology and morphometry

Following the initial shortlisting of the skylight candidates based upon morphology, we have carried out their detailed morphometric examination. For this, we have estimated their true vertical depth at the point located at the edge of the shadow. The depth (D) of the skylight candidates have been estimated from the length of shadows ($L_s$), the solar incidence angle (i), and the emission angle (e) at the time of the observation, using the approach of Cushing et al. (2015). Formulas, $D= L_s/ [\tan (i)-\tan (e)]$ and $D=L_s \cos(i) \cos(e)/ [\sin (i+e)]$ have been used to calculate the depth of the skylight candidates for Phase Angle <i and Phase Angle >i, respectively. Here, the length of the visible shadow ($L_s$) is the horizontal distance in the direction of illumination from the shadow-casting point on the rim to the edge of the shadow cast upon the floor, and depth (D) is the true vertical depth at that point. The skylight candidates are classified as Bowl-shaped Pit Craters (BPCs) and Atypical Pit Craters (APCs) based on their Depth to Length Ratio ($D_{LR}$), which is defined as $D/L_{max}$. The skylight candidates are classified as BPCs if $0.1 \leq D_{LR} \leq 0.3$ and APCs if $0.3 < D_{LR} < 2.5$ (Cushing et al., 2015).

Further, the APCs are classified into three morphological types based upon $D_{LR}$ values and morphological characteristics. For the morphological types, APC I, APC II, and APC III, the $D_{LR}$ values are > 0.6, 0.4-0.8, and ~0.25-0.5, respectively (Cushing et al., 2015). According to Cushing et al. (2015), the APC I type candidates are bell-shaped and they possess overhanging walls and rims. The overhanging rim is thinner on the surface and thicker with increasing depth. If the overhang is symmetrical around the pit, the diameter of the cave floor may be approximately double that of the surface aperture. The APC II candidates show near-vertical walls for the upper part and overhanging wall in the lower part. The APC IIIs possess near-vertical walls with the absence of the overhanging walls. Mostly, the APC I possess a flat cave floor and the talus material is absent in it. The APC II has a bowl-shaped cave floor with the presence of talus material and APC III has a flat cave floor with dust-covered rubble. Thus, the lateral extent of the overhanging walls decreases in APC II in comparison to APC I. It is to be noted that APC II may be misinterpreted as APC III in nadir observations unless the presence of overhangs at the base of pit walls is evident. Similar to the APCs, the BPCs have also been classified into three types based upon their $D_{LR}$ values and shape (Cushing et al., 2015). For morphological types BPC I, BPC II and BPC III the $D_{LR}$ values are $0.3 \geq D_{LR} > 0.25$, $0.25 \geq D_{LR} > 0.2$ and $0.2 \geq D_{LR} \geq 0.1$, respectively. For BPC I, BPC II, and BPC III, the shapes are near bowl-shaped, bowl-shaped, and shallow bowl-shaped, respectively.

Another important morphometric indicator is Elongation Index (EI), which is the ratio between the longest axis ($L_{max}$) and the width ($W_{max}$) perpendicular to it. The Elongation Index (EI), which defines the shape of the skylight candidates, is a measure of the degree of modification that the candidate skylights have undergone since their formation. The EI of the perfect circle is 1. For shapes circular and sub-circular, elliptical, sub-elliptical, and elongated, the values are $1 < EI \leq 1.21$, $1.21 < EI \leq 1.65$, $1.65 < EI \leq 1.8$, and $EI > 1.8$, respectively (Kobal et al., 2014). The EI indicates the degradation state of the potential cave roof which may be sometimes related to the age of the skylight structure. Primarily, the EI value of the older skylight is markedly high because the potential cave roof degrades over time and collapses. Over time, the dust also falls to the cave floor. Due to these reasons, the original $D_{LR}$ value at the time of formation decreases.

### 3.2.2 Geological Context

Besides the morphometric characterization of the skylight candidates, we have also classified them based on their formation mechanism and geological context. The nature of the origin of the skylight in this study should be mostly volcanic or tectonic since they are situated on the flank of Elysium Mons. During volcanism, there is a movement of magma in the subsurface and lava on the surface. Both these activities can result in the formation of skylights due to different processes.

(i) Lava Tubes (LT) - The less viscous lava flows on the surface. The upper layer of the lava flow cools relatively faster. Therefore, the top layer hardens, which results in the formation of a tube. The rapid flow of lava through the tube decreases with time and finally, the tube is left with no lava flow. The empty tube would have hard boundaries and space inside. When the roof of this tube collapses, a skylight is formed which provides access to the lava tube cave.

(ii) Horizontal Magma Conduit (HMC) –The horizontal propagation of magma through flank dikes form a horizontal magma conduit. The subsurface flow of magma forms the underground tubes. The overhead material of this tube can fall due to tectonic activities which results in the formation of a skylight that is connected to the subsurface tube. In this case, only the skylight would be visible and no tube would be observed on the surface.

(iii) Volcanic-Tectonic Feature (VTF) - The region with a high influx of subsurface magma flow would have large tectonic activities that result in the formation of rift zones. The strong tectonic activities in the rift zone can produce faults and grabens. In these cases, the skylights are associated with visibly discernable tectonic features on the surface. On most occasions, these skylight candidates form a chain.

The skylight candidates have been classified as Lava Tube (LT) skylight when they are associated with lava tubes, and as Volcanic-Tectonic Feature (VTF) skylight when they are associated with fractures, faults or graben. If the skylight candidates are located on a volcanic flank but are not associated with any of these features, they are classified as Horizontal Magma Conduit (HMC) skylight. In general, the APCs are potential skylights connected to caves; however, under certain circumstances when the BPCs are associated with Lava tubes and Horizontal Magma Conduits, they can also be potential skylights (Cushing et al., 2015).

### 3.3 Determination of potential cave entrance

Determining potential cave entrance is very useful for future manned/ robotic exploration of the red planet Mars. In the HiRISE images, the darker black area represents greater depths where the sunlight is barely reaching. In this region, there is a high probability of having a cave entrance. In general, the skylights exhibit potential cave entrance appearance as a dark linear part in the subset of the darker region by stretching the image contract (Cushing et al., 2015).

## 4.0 Results and discussion:

### 4.1 Identification of skylight candidates

In this study, we have examined a total of thirty-two skylight candidates (SK1-32) on the flank of the Elysium Mons. Their location, elevation, morphometric characteristics, and geological context are listed in Table1. Among them, twenty-six candidates (SK1-6, 8-9, 13-22, 24-25, and 27-32) are newly found ones and the remaining six (SK7, 10-12, 23, and 26) (Fig. 3, 7) are from the Mars Cave database of Cushing and Okubo (2015), and Cushing (2019). An example from this study is shown in Fig. 2. In the middle part of the image, there is a skylight candidate (SK 15). It can be seen that the impact craters in the adjoining areas exhibit crater rays, ejecta, and elevated rim, but the candidate skylight does not show any of these features (Fig. 2 (a)). Again, while in the THEMIS brightness temperature image of evening time, the candidate skylight and impact craters look-alike (Fig. 2 (b)), the skylight candidate shows warmer appearance than the impact craters and the surrounding areas at midnight (Fig. 2 (c)). Further, it has been found that the SK15 is 4.9K warmer than the surrounding area in the daytime whereas it is 15.3K warmer than the surrounding area in the nighttime. The diurnal amplitude of temperature variation for SK15 is 10.4 K, which is much lower than the diurnal amplitude of temperature variation of the surrounding area (Fig. 2 (c)).

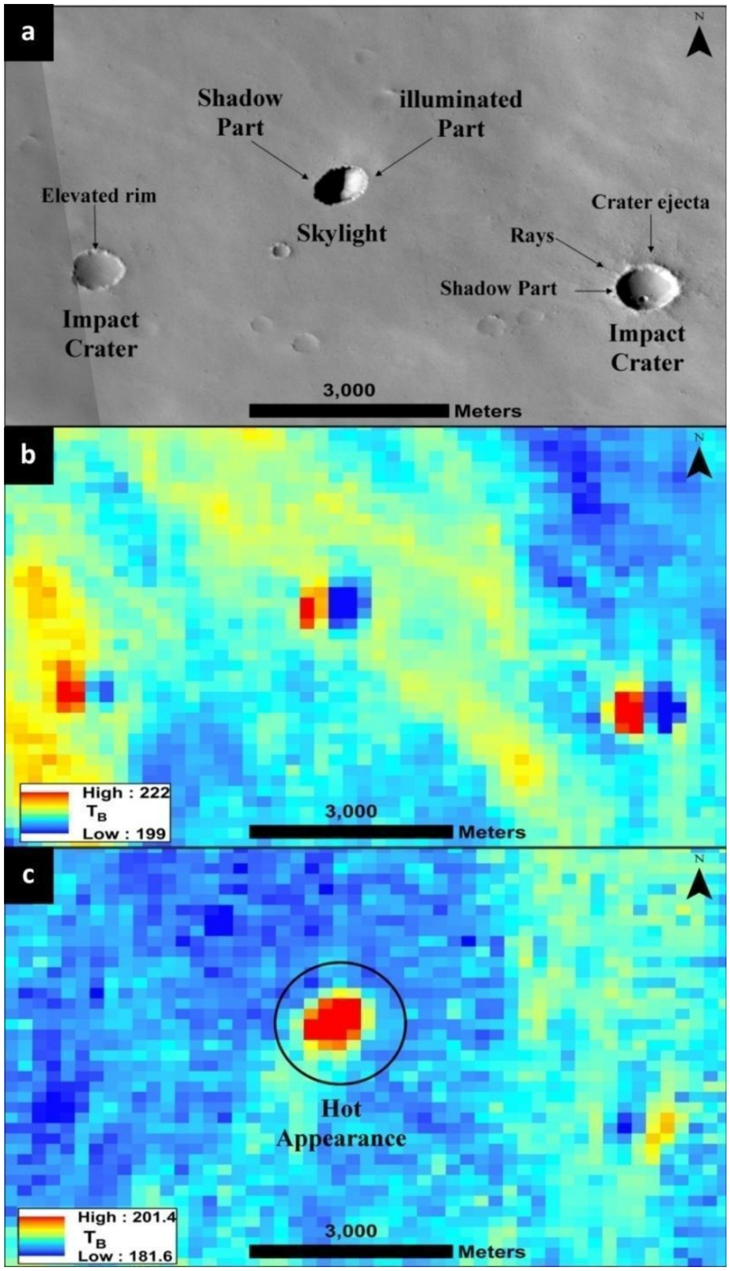


**Figure 2: (a)** A CTX daytime image acquired at 10:33 AM; **(b)** An IRPBT image acquired during the evening at 5:22 PM. **(c)** An IRPBT image acquired at midnight around 11:34 PM.

**Table 1:** The morphometry and classification of the skylight candidates on the flank of the Elysium Mons studied here. Here, SK, EI, $D_{LR}$, BPC, APC, GU, Hve, IHvf, AHv, AGF, LT, and TF refers to Skylight candidate, elongation Index (EI = $L_{max}/W_{max}$), depth to length ratio ($D_{LR}$ = $D/L_{max}$), Bowl-shaped Pit Crater, Atypical Pit Crater, geological units from Tanaka et al. (2014)

[Hesperian volcanic edifice, Late Hesperian volcanic field, Amazonian and Hesperian volcanic unit], associated geological features, lava tube, and tectonic features respectively. Here, if the associated geological feature for a skylight candidate is "None", it can be associated with a subsurface Horizontal Magma Conduit (HMC). Additional information, attributes of the skylight candidates such as Perimeter (Pe), maximum length ($L_{max}$), and maximum width ($W_{max}$) are tabulated in Table ST1. The thermal attributes of the skylight candidates such as IRPBT image id, $T_{max,}$ and $T_{mean,}$ are tabulated in Table ST2.

| Identification no., Location, and Elevation | | | Morphometry Observation | | | Geological Context | |
|---|---|---|---|---|---|---|---|
| SK | Latitude<br>Longitude | Elevation (m) | EI | $D_{LR}$ | BPC/APC and type | GU | AGF |
| 1 | 24.4781<br>147.1324 | 11556 | 1.2 | 0.30 | BPC I | Hve | LT |
| 2 | 24.4488<br>147.1139 | 11495 | 1.1 | 0.20 | BPC III | Hve | None |
| 3 | 24.4458<br>147.1225 | 11436 | 1.1 | 0.30 | BPC I | Hve | None |
| 4 | 24.7341<br>147.3604 | 9912 | 1.1 | 0.32 | APC III | Hve | LT |
| 5 | 24.4439<br>147.4351 | 9265 | 1.1 | 0.25 | BPC II | Hve | None |
| 6 | 24.5934<br>147.4581 | 9208 | 1.0 | 0.31 | APC II | Hve | None |
| 7 | 24.7541<br>147.5137 | 8919 | 1.0 | 0.59 | APC II | Hve | None |
| 8 | 24.7602<br>147.5456 | 8706 | 1.0 | 0.14 | BPC III | Hve | None |
| 9 | 24.7667<br>147.5712 | 8472 | 1.0 | 0.25 | BPC III | Hve | None |

| | | | | | | | |
|---|---|---|---|---|---|---|---|
| 10 | 24.4158<br>150.6179 | 4050 | 1.0 | 0.17 | BPC III | Hve | None |
| 11 | 22.5202<br>149.8417 | 2368 | 1.1 | 0.35 | APC III | Hve | None |
| 12 | 23.2104<br>151.7289 | 2034 | 1.0 | 0.48 | APC II | AHv | None |
| 13 | 26.3785<br>144.1544 | 1828 | 1.4 | 0.29 | BPC III | Hve | None |
| 14 | 26.8415<br>142.2201 | 1072 | 1.7 | 0.20 | BPC III | IHvf | None |
| 15 | 27.6947<br>142.1096 | 710 | 1.3 | 0.40 | APC II | AHv | TF |
| 16 | 22.9848<br>152.2478 | 186 | 1.5 | 0.27 | BPC I | AHv | None |
| 17 | 22.9114<br>152.3603 | 129 | 1.3 | 0.42 | APC III | AHv | None |
| 18 | 22.9058<br>152.3724 | 124 | 1.7 | 0.40 | APC III | AHv | None |
| 19 | 25.1059<br>144.6727 | 2468 | 1.1 | 0.14 | BPC III | Hve | None |
| 20 | 25.0977<br>144.6739 | 2462 | 1.0 | 0.21 | BPC III | Hve | None |
| 21 | 25.0892<br>144.6751 | 2447 | 1.0 | 0.19 | BPC III | Hve | None |
| 22 | 25.0786<br>144.6775 | 2438 | 1.1 | 0.24 | BPC II | Hve | None |
| 23 | 29.2600<br>145.6594 | -224 | 1.0 | 2.53 | APC I | AHv | None |
| 24 | 25.5711<br>146.4503 | 7512 | 1.0 | 0.41 | APC II | Hve | None |

| | | | | | | | |
|---|---|---|---|---|---|---|---|
| 25 | 19.8542<br>141.8167 | 667 | 1.0 | 0.23 | BPC I | AHv | None |
| 26 | 30.5613<br>146.498 | -1522 | 1.1 | 0.33 | APC III | AHv | None |
| 27 | 30.585<br>140.238 | -2193 | 1.0 | 1.18 | APC I | AHv | TF |
| 28 | 30.5963<br>140.2247 | -2220 | 1.8 | 0.59 | APC I | AHv | TF |
| 29 | 30.9681<br>140.2599 | -2532 | 1.1 | 1.09 | APC I | AHv | None |
| 30 | 30.9834<br>140.3423 | -2547 | 1.4 | 0.80 | APC I | AHv | None |
| 31 | 31.0412<br>140.5132 | -2551 | 1.1 | 0.86 | APC I | AHv | None |
| 32 | 31.0132<br>140.3454 | -2555 | 1.2 | 0.58 | APC II | AHv | None |

Among the thirty-two skylight candidates examined in this study, SK1-23 showed a warmer appearance than the surrounding area at the nighttime. Among these, the SK1-9, 11-12, and 14-15 appeared warmer than the surrounding area during the daytime as well; however, the amplitude of variation was found to be lower for the skylight candidates in comparison to their surroundings. For skylight candidates, SK10, 13, and 16-23, daytime thermal analysis was not carried out as their afternoon thermal (~13:00-14:00) data was not available. The thermal criteria for the skylight candidates SK24-32could not be verified due to their very small size i.e. less than 100m.

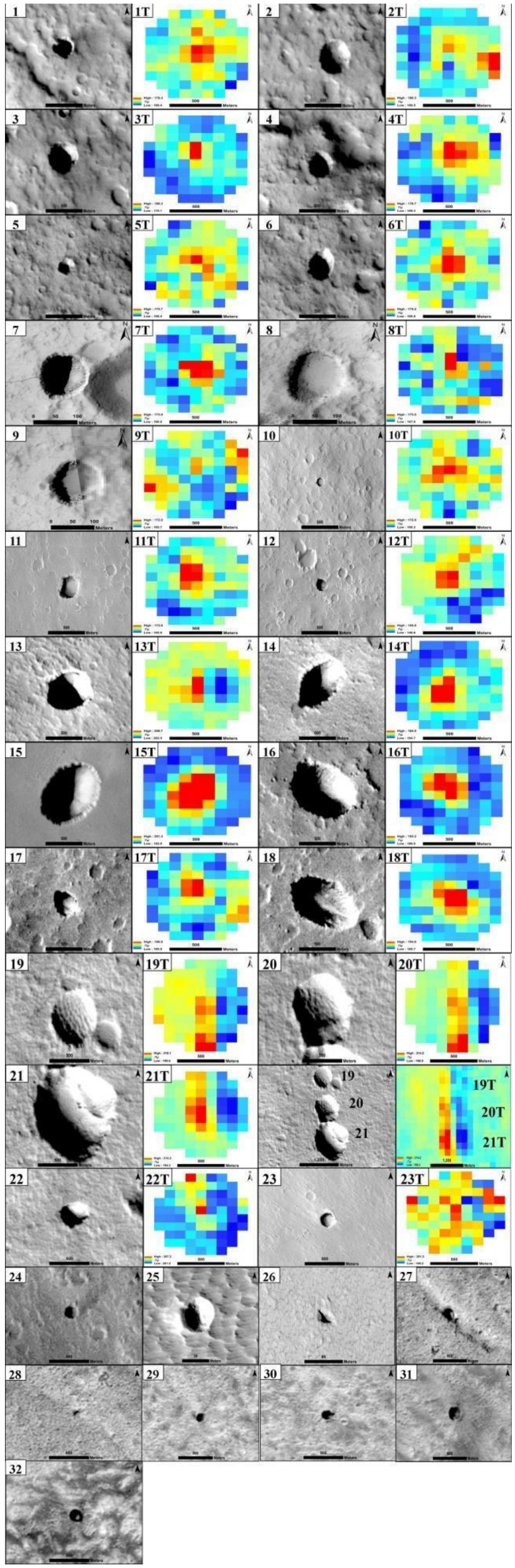
1
1T
2
2T
3
3T
4
4T
5
5T
6
6T
7
7T
8
8T
9
9T
10
10T
11
11T
12
12T
13
13T
14
14T
15
15T
16
16T
17
17T
18
18T
19
19T
20
20T
21
21T
19
20
21
19T
20T
21T
22
22T
23
23T
24
25
26
27
28
29
30
31
32

293

**Figure 3:** A view of the thirty-two candidate skylights using CTX/HiRISE images. The corresponding THEMIS IRPBT images are shown for the candidates (SK1-23). The SK24-32 are less than 100m in diameter therefore their thermal behavior could not be studied. The candidates SK1-23 show a warmer appearance than the surrounding area (a circular buffer zone of radius 500 m) around midnight (11:30 pm to 2:00 am) in the northern summer season (Ls =90-180). Since the midnight data was not available for four candidates (SK 12, 16-18) therefore, they have been observed around 9-10 pm.

## 4.2 Classification of Skylight candidates

### 4.2.1 Morphometry

Based on the $D_{LR}$ values, seventeen candidates (SK 4, 6, 7, 11, 12,15, 17, 18, 23, 24, and 26-32) have been found to exhibit $0.3 < D_{LR} < 2.5$, therefore, they have been classified as Atypical Pit Craters (APCs). The rest of them i.e. fifteen skylight candidates (SK 1-3, 5, 8-10, 13, 14, 16, 19-22, and 25) exhibits $0.1 \leq D_{LR} \leq 0.3$; therefore, they fall in the category of Bowl-shaped Pit Craters (BPCs). These have been further classified into their morphological types based on the $D_{LR}$ values (Table 1), as mentioned in section 3.2.1. The APCs SK (23 and 27-31) have been classified as APC I, SK (6, 7, 12, 15, 17, 18, 24, and 32) as APC II, and SK (4, 11, and 26) as APCIII. The BPCs SK (1, 3, 16, and 25) have been categorized as BPC I, SK (5 and 22) as BPC II, and SK (2, 8-10, 13, 14, and 19-21) as BPC III.

Further, it can be noted in Table 1 that the EI value of 75% of the skylight candidates SK(1-12, 19-27, 29, 31, and 32) correspond to circular to sub-circular shape, indicating that their roof has remained more-or-less stable since their formation. The EI of the rest of the candidates i.e., 25% of the population considered in this study, SK (13-18, 28 & 30), correspond to elliptical to sub-elliptical shape, indicating the possibility that they would have experienced roof collapse over time. Among the elliptical APCs, it has been found that SK15 (EI:1.3) and SK 28(EI:1.8) are indeed located around tectonic fractures (Fig. 4) that would have promoted the roof collapse. With the increase in the EI value due to roof collapse, the amount of the talus material also increases on the floor resulting in a decrease of $D_{LR}$ value.

The $D_{LR}$ value of a skylight candidate could also be indirectly related to the age of the geological formation which possesses it. A skylight candidate association with old aged, say Hve (Hesperian volcanic edifice), does not prove an old age for the skylight candidate itself. Nevertheless, it supports the possibility that the skylight candidate could as well be contemporaneously old. With the increase in the life-span of a candidate skylight, the possibility of dust in-filling and roof collapse also increases, which will result in a reduced $D_{LR}$ value of the concerned candidate. An assessment of the association of the APCs and the BPCs characterized in this study with the geological terrains of Tanaka et al. (2014) reveals that they are located on three units Hve, lHvf, and AHv. Most of the APCs are located on the youngest AHv unit (except for SK 4, 6, 7, 11, and 24); whereas, the BPCs are largely concentrated on the Hve terrain (except for SK 16 and 25). One of the BPCs SK 14 is lying on an intermediate aged volcanic formation lHvf.

Further, the dust found on the floor of the potential cave also depends on the amount of dust present in the surrounding area. For example, we observe that the APCs SK 29-32 are associated with a large crater (Fig. 4 (d)). Hence, it is can be conveniently inferred that an extra amount of dust in the form of crater ejecta would have gone into it. The BPC SK 25 is surrounded by dune (Fig. 4 (f)) which increases the possibility of dust filling into it. The SK 25 appears to be a rock shelter which is a natural cavity enclosed by one or more rock walls and an overhang. It is observed that they have a flat potential cave floor with dust-covered rubble (Fig. 5). Thus, it is apparent that the $D_{LR}$ value is affected by parameters such as associated geological features and the age of the skylight candidate/ the host surface. Besides, morphological evidence of roof collapse has also been noticed in the BPCs (Fig. 3 and 5). With time, the following sequence APC I → APC II → APC III → BPC I → BPC II → BPC III can be observed. These results indicate that the skylight candidates classified as BPCs in this study may also be associated with subsurface caves similar to the APCs. Morphologically, SK 1 shows resemblance to APC I, SK 3 as APCI or APC II, and SK 5, 8-10, 13, 22 show resemblance to APC II, and SK 2, 14, 16, 19, 20, 21, 25 show resemblance to APC III.

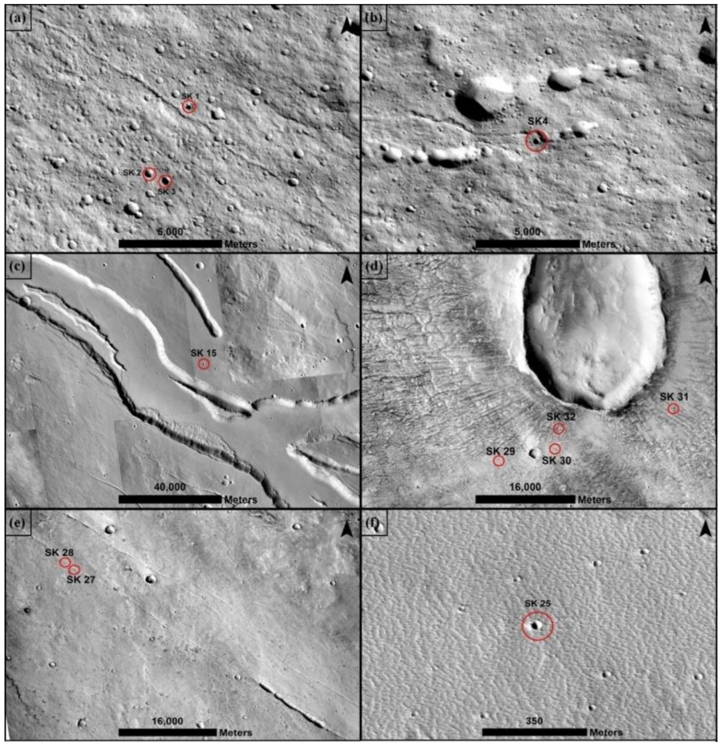


**Figure 4:** A view of the geological features associated with skylight candidates. (a) A rille associated with SK1 and presence of SK2 and SK3 in the nearby area; (b) A rille associated with SK 4; (c) A graben associated with SK15; (d) a large crater associated with SK29, 30, 31, and 32; (e) A tectonic fracture associated with SK 27 and SK28; and (f) Dune associated with SK25.

#### 4.4.2. Geological context

This study shows that only five skylight candidates SK 1, 4, 15, 27, 28 are associated with geological features (Table 1). The skylight candidates SK 1 and 4 are associated with rille structure (Fig.4 a, b), whereas the candidates SK 15, 27, and 28 are associated with Volcanic Tectonic Features (Fig.4 c, e). The others are not associated with any of the geological features therefore they may be related to Horizontal Magma Conduits (HMC). E.g., three skylight candidates SK7, SK8, and SK9 are arranged in a linear array (Fig. 6). It is very much possible that they may be related to the horizontal spread of magma through a flank dike.

### 4.5 Determination of Potential Cave entrance

The determination of potential cave entrance is possible using HiRISE images due to its very high spatial resolution. In this study, investigation for potential cave entrance has been attempted for nine candidates for which HiRISE images were available. As shown in Fig. 5, a subset of the shadowed part in the contrast stretched HiRISE images is delineated by the red boundary. The darker area in this subset indicates deeper locales where the sunlight is barely reaching. In this region, there is a high probability of the presence of a cave entrance. The SK 7-12 and 23 exhibits potential cave entrance in the form of a dark linear part indicated by a red arrow (Fig. 5). The gray and relatively white areas are shallower regions on the potential cave floor where the scattered sunlight is reaching. The reduction of depth in these areas of the potential cave floor may be due to the presence of talus and/or dust material of varying thicknesses. The white areas have a thicker pile compared to the gray areas. In most of these cases, the white area is also found at the edges of the subset since the light directly reaches the edges or the side of the upper walls.

The SK 25 and SK 26 exhibits potential cave entrance in the form of a continuous shadowed pattern. The white pattern is visible at the edges of the upper walls with a continuous shadow pattern on the potential cave floor which indicates that the upper roof of the rock shelter has suddenly collapsed or a huge amount of dust had fallen. In SK 23, heavy talus material has been observed as a white pattern in the west and south-west direction while gray shade indicates irregular collapse material on the potential cave floor during different times. The SK8 and SK 11 have a pile of talus material in the SW and western direction denoted by a white dotted scattered pattern. Comparatively less, SK9 has a pile of talus material in the NW and western directions. In SK 11, the darker region has been present in NW and West direction as it is indicative of higher depth while the subset of the darker region in an enclosed box on the left side is indicative of the irregular pile of talus material and dust at the potential cave floor within overtime. Thus, the HiRISE image investigation also indicates the evolutionary stage of a skylight candidate by providing evidence for the presence of dust and talus material on the potential cave floor. The HiRISE image investigation here provides support that the BPCs (SK 8-10, and 25) could also be potentially connected to caves similar to the APCs.

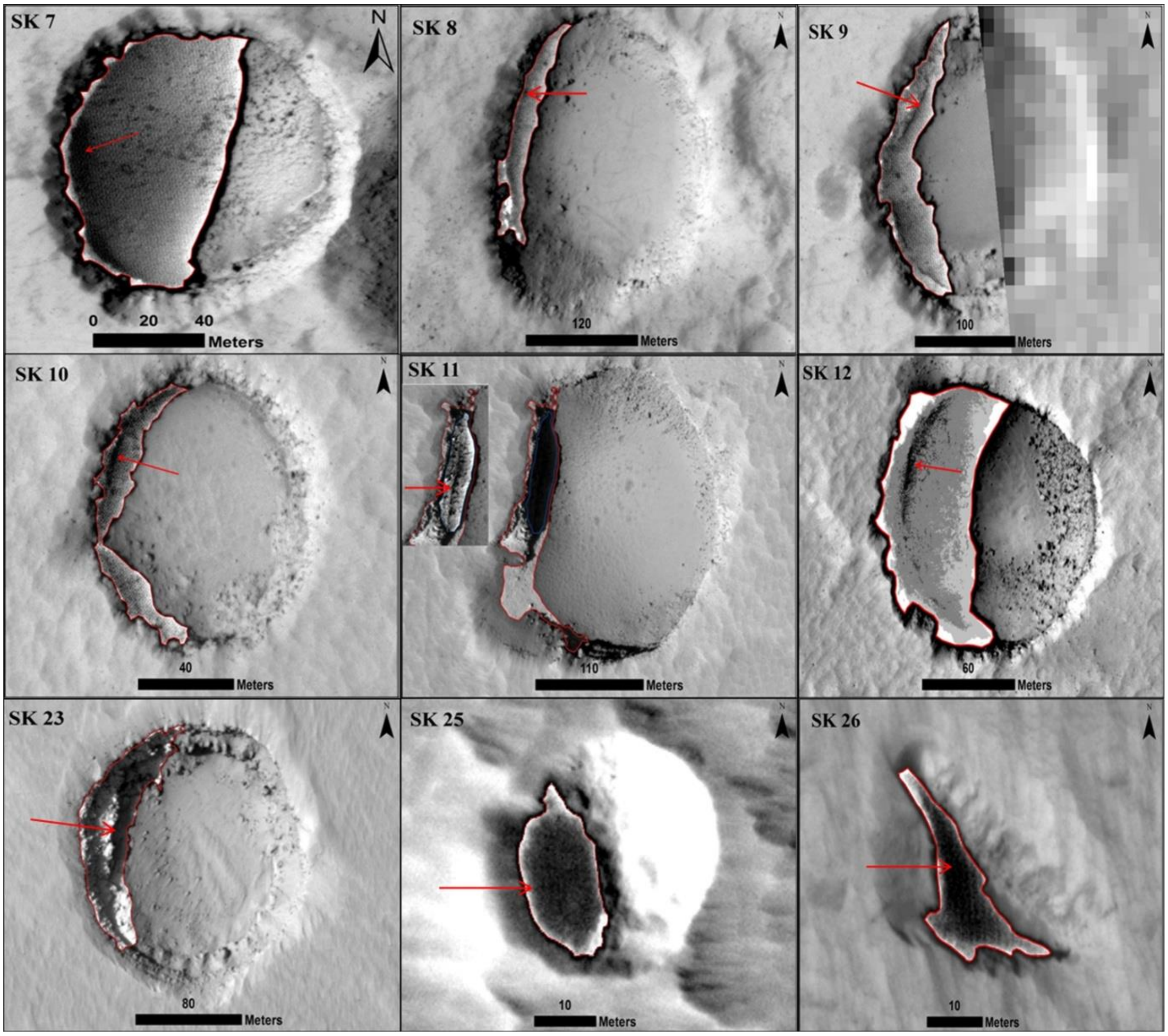


**Figure 5:** The contrast stretched HiRISE images of skylight candidates (SK7-12, 23, 25, and 26). The shadowed area in the original panchromatic images is enclosed by a red polygon. The red-colored arrows show the potential entrance for the associated potential caves in each of these cases.

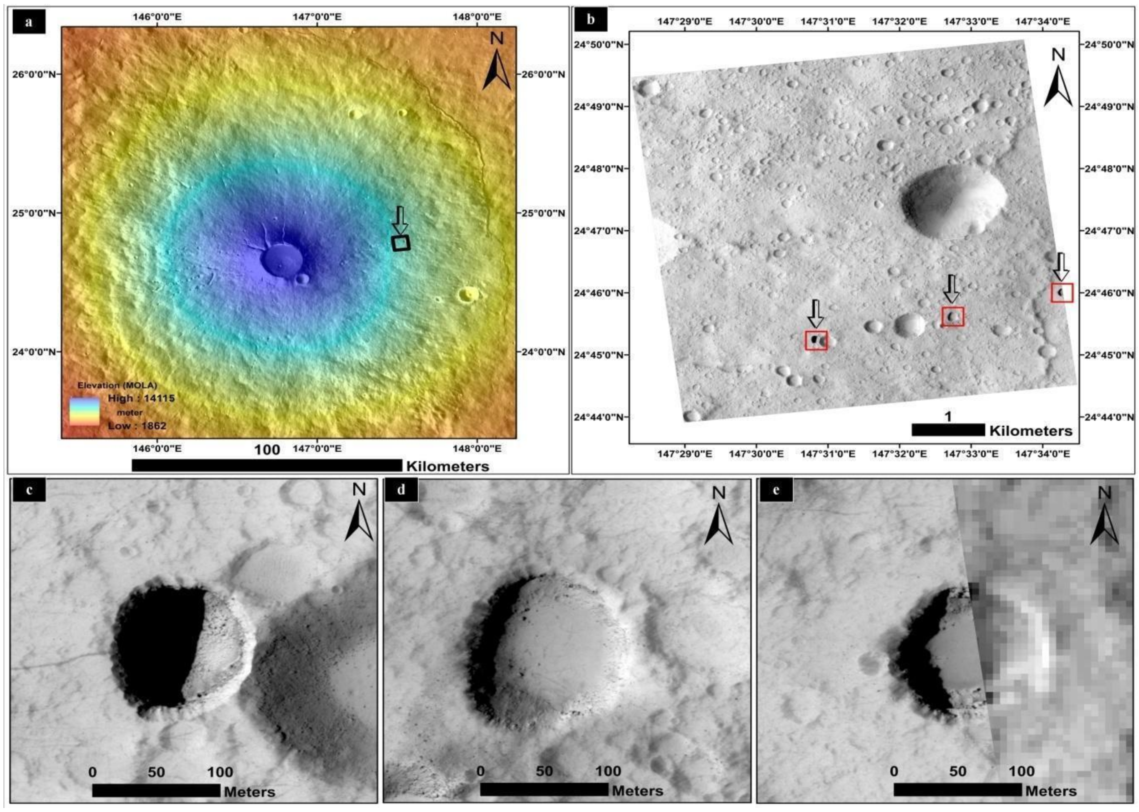


**Figure 6:** (a) An elevation map of the Elysium Mons region using MOLA and THEMIS IR day images in the background showing the location of the skylight candidates (SK7, SK8, and SK9); (b) A close-up view of the area enclosed by the black box in subsection (a). Here, the individual skylight candidates are enclosed by a red box; (c-e) A close-up view of the individual skylight candidates. The sub-sections (c) & (d) have been prepared using HiRISE images while a combination of HiRISE (left side) and CTX (right side) data has been used for depicting a close-up view of the third skylight candidate (e).

## Conclusions

In this study, thirty-two skylight candidates on the flank of Elysium Mons on Mars (Fig 7) have been examined for morphology, morphometry, and thermal behavior. Out of these, twenty-six candidates, identified here as SK (1-6, 8-9, 13-22, 24-25, and 27-32), are newly identified ones. Among all, based upon their depth to length ratio, seventeen skylight candidates SK(4,6-7, 11-12, 15, 17-18, 23-24, and 26-32) have been classified as Atypical Pit Craters

(APCs), and fifteen skylight candidates (SK1-3, 5, 8-10,13-14, 16, 19-22, and 25) as Bowl-shaped Pit Craters (BPCs). These include twelve newly discovered APCs (SK4, 6, 15, 17-18, 24, and 27-32) and fourteen newly discovered BPCs (SK1-3, 5, 8-9, 13-14, 16, 19-22, 25). The APCs are considered as potential skylights. However, our study shows that how APCs evolve with time, and under certain conditions, such as geological context and time of formation, the BPCs can also be considered as potential skylights. Some of these sites could be important destinations for any future robotics/human explorations of the Red Planet Mars.

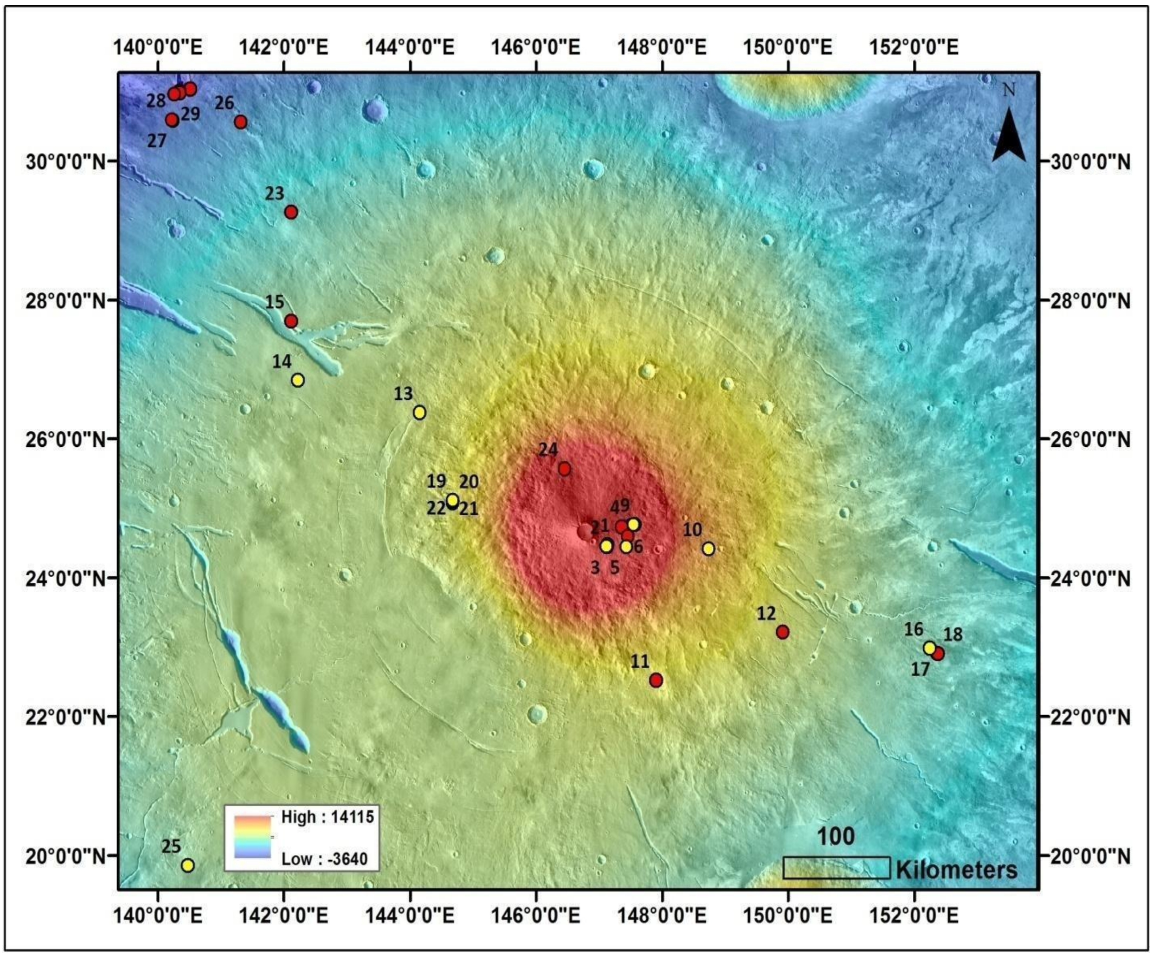


**Figure 7:** An elevation map of Elysium Mons, Mars from MOLA data showing the location of the thirty-two skylight candidates studied here. The red dots and yellow dots correspond to those classified as APCs SK (4,6-7,11-12,15,17-18,23-24, and 26-32) and BPCs SK (1-3,5,8-10,13-14,16,19-22 & 25), respectively. Out of thirty-two skylight candidates, twenty-six SK (1-6, 8-9, 13-22, 24-25, and 27-32) are newly discovered ones.

## 6. Acknowledgments

We gratefully acknowledge scientific teams for providing data of HiRISE and CTX camera from MRO (Malin et al., 2007) and THEMIS IRPBT data from Mars Odyssey (Christensen et al., 2004; 2017) downloaded through the publically accessible web portal - Mars Orbital Data Explorer (ODE) (https://ode.rsl.wustl.edu/mars/) produced by the PDS Geosciences Node at Washington University in St. Louis. We also acknowledge MOLA team for providing data from MGS (Smith et al., 2001; 2003) (Global MOLA mosaic data download link - ftp://pdsimage2.wr.usgs.gov/pub/pigpen/mars/mola/mola128_88Nto88S_Simp_clon0.zip), Mars Cave Catalog from Cushing and Okubo (2015) and Cushing (2019) (https://www.sciencebase.gov/catalog/item/5bd36eb1e4b0b3fc5ce51783), and geological units layers from Tanaka et al. (2014) (http://pubs.usgs.gov/sim/3292), an image data from MOLA team, NASA Goddard Space Flight Centre (2003) (https://www.lpi.usra.edu/science/treiman/greatdesert/workshop/marsmaps1/). We would like to thank Varun Sheel, S.A. Haider, and Anil Bhardwaj, Director PRL, Ahmedabad, India for providing encouragement and necessary facility to carry out this work.

## 7. References

Antoine, R., Baratoux, D., Rabinowicz, M., Fontaine, F., Bachèlery, P., Staudacher, T., and Finizola, A. (2009), Thermal infrared image analysis of a quiescent cone on Piton de la Fournaise volcano: Evidence of convective airflow within an unconsolidated soil, Journal of Volcanology and Geothermal Research, Vol. 183, Issues 3-4, Pages 228-244, ISSN 0377-0273, https://doi.org/10.1016/j.jvolgeores.2008.12.003

Antoine, R., Lopez, T., Baratoux, D., Rabinowicz, M., and Kurita, K. (2011), Thermal analysis of fractures at Cerberus Fossae, Mars: Detection of air convection in the porous debris apron, Icarus, 214, 2, 433-446, ISSN 0019-1035. https://doi.org/10.1016/j.icarus.2010.12.025

Bairagya, H. (2014), Environmental conditions of Borra Cave, Visakhapattanam, India. International Journal of Environment, 3, 2, 150-166. https://doi.org/10.3126/ije.v3i2.10526

Boston, P.J., Frederick, R.D., Hildreth-Werker, V., Sprungman, B., Thompson, S.L. and Welch, S.M. (2003a), "Human Utilization of Subsurface Extraterrestrial Environments: Final Report", NIAC – Caves of Mars, K26-01535. https://digital.lib.usf.edu/?k26.1535

Boston, P.J., Frederick, R.D., Welch, S.M., Werker, J., Meyer, T.R., Sprungman, B., Hildreth-Werker, V., Thompson, S.L., and Murphy, D.L. (2003b), Human utilization of subsurface extraterrestrial environments, Gravitational and Space Biology Bulletin: Publication of the American Society for Gravitational and Space Biology, 16, 2, 121-131, PMID: 12959139. https://europepmc.org/article/MED/12959139

Boston, P.J., Frederick, R.D., Welch, S.M., Werker, J., Meyer, T.R., Sprungman, B., Hildreth-Werker, V., and Thompson, S.L. (2004), Extraterrestrial subsurface technology test bed: Human use and scientific value of Martian caves, In AIP Conference Proceedings 699, 1, 1007-1018. https://doi.org/10.1063/1.1649667

Christensen, P. R., Jakosky, B. M., Kieffer, H. H., Malin, M. C., McSween, H. Y., Nealson, K., et. al. (2004), The Thermal Emission Imaging System (THEMIS) for the Mars 2001 Odyssey Mission, Space Science Reviews, 110, 1-2, 85-130. https://doi.org/10.1023/B:SPAC.0000021008.16305.94

Christensen, P.R., THEMIS Principal Investigator and Arizona State University (2017), 2001 Mars Odyssey Thermal Emission Imaging System (THEMIS), Data Processing User's Guide Part 1 – Infrared, Version 0.23, page 1-21. https://static.mars.asu.edu/pds/ODTSDP_v1/calib/process_ir.pdf

Cushing, G. E., Titus, T.N., Wynne, J. J., and Christensen, P. R. (2007), THEMIS observes possible cave skylights on Mars, Geophysical Research Letters, 34, L17201. https://doi.org/10.1029/2007GL030709

Cushing, G. E. (2012), Candidate cave entrances on Mars, Journal of Cave and Karst Studies, 74, 1, 33-47. https://doi.org/10.4311/2010EX0167R

Cushing, G. E., Okubo, C. H., and Titus, T. N. (2015), Atypical Pit Craters on Mars: New insights from THEMIS, CTX, and HiRISE observations, Journal of Geophysical Research: Planets, 120, 1023-1043. https://doi.org/10.1002/2014JE004735

Cushing, G. E., and Okubo, C. H. (2015), The Mars Cave Database, 2nd International Planetary Cave Conference, LPI Contribution No. 1883, p.9026, Bibcode: 2015LPICo1883.9026C https://www.hou.usra.edu/meetings/2ndcaves2015/pdf/9026.pdf

Cushing, G. (2019), Mars Cave Catalog, USGS Astrogeology Science Center. https://www.sciencebase.gov/catalog/item/5bd36eb1e4b0b3fc5ce51783

Hill, C. A., and Forti, P. (1997), Cave minerals of the world (Second edition), Huntsville: National Speleological Society, 463 pages, ISBN: 9781879961074, 1879961075

Jung, J., Yi, Y., & Kim, E. (2014), Identification of Martian cave skylights using the temperature change during day and night, Journal of Astronomy and Space Sciences, 31, 2, 141-144. https://doi.org/10.5140/JASS.2014.31.2.141

Kobal, M., Bertoncelj, I., Pirotti, F., and Kutnar, L. (2014), Lidar Processing for Defining Sinkhole Characteristics under Dense Forest Cover: A Case Study in the Dinaric Mountains, ISPRS - International Archives of the Photogrammetry, Remote Sensing and Spatial Information Sciences, Volume XL-7, 113-118. https://doi.org/10.5194/isprsarchives-XL-7-113-2014

Lopez, T., Antoine, R., Baratoux, D., Rabinowicz, M., Kurita, K., and d'Uston, L. (2012), Thermal anomalies on pit craters and sinuous rilles of Arsia Mons: Possible signatures of atmospheric gas circulation in the volcano, Journal of Geophysical Research: Planets, 117, E09007. https://doi.org/10.1029/2012JE004050

Malin, M. C., Bell, J. F., Cantor, B. A., Caplinger, M. A., Calvin, W. M., Clancy, R. T., Edgett, K. S., Edwards, L., Haberle, R.M., et. al. (2007), Context camera investigation onboard the Mars

Reconnaissance Orbiter, Journal of Geophysical Research: Planets, 112, E05S04. https://doi.org/10.1029/2006JE002808

Mars Orbital Data Explorer (ODE), produced by the PDS Geosciences Node at Washington University in St. Louis. https://ode.rsl.wustl.edu/mars/

MOLA team, NASA Goddard Space Flight Center (2003), A MOLA data derived elevation map of Mars, https://www.lpi.usra.edu/science/treiman/greatdesert/workshop/marsmaps1/

Romero, A. (2009), Cave biology: life in darkness, Cambridge University Press, ISBN 9780511596841, https://doi.org/10.1017/CBO9780511596841

Sharma, R., Srivastava, N., & Yadav, S. K. (2019), Resource potential and planning for exploration of the Hebrus Valles, Mars, Research in Astronomy and Astrophysics, 19(8), 116. https://doi.org/10.1088/1674-4527/19/8/116

Smith, D. E., Zuber, M. T., Frey, H. V., Garvin, J. B., Head, J. W., Muhleman, D. O., et al. (2001), Mars Orbiter Laser Altimeter: Experiment summary after the first year of global mapping of Mars, Journal of Geophysical Research: Planets, 106(E10), 23689-23722. https://doi.org/10.1029/2000JE001364

Smith, D.E., Zuber, M.T., Neumann, G.A., Guinness, E.A., and Slavney, S. (2003), Mars Global Surveyor Laser Altimeter Mission Experiment Gridded Data Record, MGS-M-MOLA-5-MEGDR-L3-V1.0, NASA Planetary Data System, 2003. (Global MOLA mosaic data download link – ftp://pdsimage2.wr.usgs.gov/pub/pigpen/mars/mola/mola128_88Nto88S_Simp_clon0.zip)

Tanaka, K.L., Skinner, J.A., Dohm, Jr., J.M., Irwin, R.P., III, Kolb, E.J., Fortezzo, C.M., Platz, T., Michael, G.G., and Hare, T.M. (2014), Geologic map of Mars, U.S. Geological Survey Scientific Investigations Map SIM 3292, scale 1:20,000,000, pamphlet 43 p., http://pubs.usgs.gov/sim/3292